Continuous Thermally Regenerative Electrochemical Systems for Directly Converting Low-Grade Heat to Electricity

Xiaoya Li[1], Jia Li[2], Jeonghun Yun[1], Angyin Wu[1], Caitian Gao[1,3], Seok Woo Lee[1, 2,*]

[1] School of Electrical and Electronic Engineering, Nanyang Technological University, Singapore 639798, Singapore

[2] Rolls-Royce@NTU Corporate Lab, Nanyang Technological University, Singapore 639798, Singapore

[3] School of Physics and Electronics, Hunan University, Changsha 410082, P.R. China

[*] Corresponding author. Email: sw.lee@ntu.edu.sg

N.B.: This is the Accepted version of this article. The final published version of the article can be found at https://doi.org/10.1016/j.nanoen.2022.107547

Abstract

Thermally regenerative electrochemical cycle (TREC) system, which converts heat to electricity by charging at a lower voltage and discharging at a higher voltage, is a promising technology with high energy conversion efficiency for low-grade heat recovery. However, its charging process consumes additional energy and breaks the continuity of power generation. Herein, we present a continuously operated TREC system for direct heat-to-electricity conversion. In this system, two identical electrochemical cells operating at different temperatures are combined in a unit; thus, electricity can be generated continuously by periodically alternating between two temperatures. This concept is mainly demonstrated with a copper hexacyanoferrate cathode and a Cu/Cu^{2+} anode, with this system achieving an energy conversion efficiency of 1.76% (14.19% of Carnot efficiency) when operated between 10 and 50 °C without heat recuperation effects. Even at an ultralow temperature difference of 10 °C vs room temperature, its efficiency is 0.98%. The proposed system allows great freedom in electrode material selection as proven by another system with nickel hexacyanoferrate cathode and Ag/AgCl anode, thereby improving the flexibility and practicability of TREC systems in low-grade heat harvesting.

Keywords: low-grade heat, energy harvesting, thermally regenerative electrochemical cycle, Prussian blue analogues, applications

1. Introduction

Low-grade thermal energy (<100 °C) is ubiquitous as waste heat in the environment, industrial power plants, and solar and geothermal fields [1,2]. Utilizing this green energy can meaningfully contribute to decarbonization; however, its distributed nature and narrow difference from the ambient temperature make its harvesting very challenging. Various thermal-to-electricity conversion technologies are being studied. Among which, solid-state thermoelectric generators (TEGs) and organic Rankine cycles (ORCs) have been extensively investigated for low-grade energy harvesting [3−5]. TEG performance is strongly limited by the small Seebeck coefficient (<0.2 mV K^{-1}) at heat source temperatures lower than 100 °C [6,7]. The feasibility of ORCs has been demonstrated for heat sources >80 °C at large power scales, but their application is limited to small or medium systems due to a lack of efficient and cost-effective expansion devices [8,9]. Liquid-state thermogalvanic cells (TGCs) have also attracted increasing attention given the high thermogalvanic coefficient, which is one order of magnitude higher than that of TEGs [10] [0].Significant advances in TGC technology have been realized via the exploration of redox couples for both sole and multiple-type TGCs [11−13]; the investigation of electrolytes for aqueous [14], non-aqueous and quasi–solid-state TGCs [15,16]; and the optimization of electrode materials [17]. However, the low energy conversion efficiency and power density of individual TGC cells and stability issues of TGC devices limit the scope of their practical applications [18]. Different from these methods, the Soret effect resulting from thermally induced ion/molecular diffusion has also been utilized to augment thermopower to several mV K^{-1} or even as high as −87 mV K^{-1} [19−21]. Such effect is more suitable for capacitor-type applications.

Recently, the thermally regenerative electrochemical cycle (TREC) system has emerged as a promising approach to low-grade thermal energy harvesting [22−25]. A high efficiency of 3.7%, corresponding to approximately 25% of the Carnot efficiency, was demonstrated in a TREC system cycled between 10 and 60 °C [22]. In a TREC, electrochemical cells are used to construct a thermodynamic cycle, typically with four steps: heating, charging, cooling and discharging. Because of the temperature dependence of cell voltage, the charging voltage at one temperature is lower than the discharging voltage at another temperature, and power can be generated from this voltage difference. The characteristic of a TREC is defined as the temperature coefficient of its electrode materials: $\alpha = \frac{\partial V}{\partial T}$. The energy conversion efficiency (η_e) of a TREC is expressed as Equation (1) [22]:

$$\eta_e = \frac{W}{Q_H + Q_{HR}} = \frac{Q_{dis}\overline{V}_{dis} - Q_{ch}\overline{V}_{ch}}{|\overline{\alpha}|T_h Q_{ch} + (1-\eta_{HR})C_p \Delta T} \quad (1)$$

where W is the net work; Q_H is the heat absorbed at high temperature T_h; Q_{HR} is the heat absorbed for raising the temperature to T_h; $\overline{\alpha}$ is the average temperature coefficient; Q_{dis} and Q_{ch} are the discharge and charge capacity, respectively; $\bar{V}_{dis}$ and $\bar{V}_{ch}$ are the average discharge voltage and charge voltage, respectively; C_p is the total heat capacity of the cells; ΔT is the temperature difference between the high and low temperatures; and η_{HR} is the heat recuperation efficiency [22]. To achieve high energy conversion efficiency, a larger temperature coefficient, lower heat capacity, and higher heat recuperation efficiency are preferred. Many efforts have been made in this regard, with a particular focus on exploring materials and underlying the mechanism [26,27], improving the temperature coefficient [28−31], reducing the cell impedance by complexing helical carbon nanotubes with the active material [32], and minimizing costs by using a membrane-free system [33].

A drawback of the TREC is that it requires external electricity for cell regeneration in the charging phase of the cycle, resulting in a discounted energy gain and discontinuities in power generation. In an ideal system, the TREC would be operated only using thermal energy, with the battery cells being regenerated only using the available heat (i.e., without external electricity). A charging-free TREC was demonstrated using an $Fe(CN)_6^{3-/4-}$ redox pair and Prussian blue as electrodes [34], but this system has strict constraints regarding the cell voltage and temperature that limit its feasibility. Specifically, to enable a polarity switch, it requires materials and electrodes that make the full-cell voltage approximately zero at some temperature and this cross-over temperature should be exactly the midpoint between the temperatures of the heat source and the heat sink. In addition, the charging-free nature of this system is realized by restricting the voltage and capacity ranges, which limits the energy output. Finally, for optimal energy harvesting, large temperature coefficients are preferred. These stringent requirements make material exploration for charging-free TREC systems difficult. Further efforts to identify suitable materials for heat sources would be case-specific and time-consuming, limiting the practicability of TREC systems. Long et al. [35] concluded continuous operation will result in higher power output and efficiency by simulation. Similar issues have been addressed in redox flow batteries and fuel cells [36]. However, there is a research gap between theoretical work and applications, which requires dedicated experiments.

Herein, we present a continuously operated TREC system for directly converting low-grade heat to electricity. The system consists of two identical electrochemical cells coupled as one unit, operated periodically at different temperatures and regenerated by alternating between the temperatures; thus, the unit is always generating a voltage output. Specifically, during each temperature alternation cycle, one cell is heated while the other is cooled. The cells discharge

spontaneously when a load is connected. By switching the temperature of the two cells, both are regenerated, and the unit outputs voltage in the reverse direction for power supply to the external load. This operation scheme avoids the need for cell regeneration breaks during operation, and thus electricity generation is continuous rather than intermittent. Moreover, the use of the electrochemical cells, which are free of moving parts, audible noises, and greenhouse emissions, enables direct conversion from low-grade energy to electricity. In this work, we experimentally demonstrate this concept mainly using a copper hexacyanoferrate (CuHCFe) cathode and a Cu/Cu^{2+} anode in a hybrid aqueous electrolyte. This system can realize energy conversion efficiencies of 1.76%, 3.08% and 5.60% when cycled between 10 and 50 °C at heat recuperation efficiencies of 0%, 50% and 80%, respectively, which correspond to 14.19%, 24.84% and 45.21% of the Carnot efficiency, respectively. The developed system has the advantages of extreme flexibility given its independence of the electrode materials (as demonstrated by another system consisting of nickel hexacyanoferrate cathode and Ag anode in KCl electrolyte), cost-effectiveness given its simple cell configuration and inexpensive components, and scalability given its straightforward operation, making it highly promising in practical applications for direct energy conversion from low-grade heat sources.

2. Material and Methods

2.1 Material synthesis and characterization.

CuHCFe was synthesized by a co-precipitation method. First, 60 mL of 40 mM $Cu(NO_3)_2$ (Strem Chemicals) and 60 mL of 20 mM $K_3Fe(CN)_6$ (Alfa Aesar) were prepared in deionized water, and both solutions were then simultaneously dropped into 30 mL of deionized water under magnetic stirring at 40 °C. A yellowish green precipitate formed after 24 h of aging. Next, the precipitate was filtered and washed by deionized water three times and by acetonitrile one time in sequence. After centrifuging, the precipitate was dried in a vacuum oven for 12 h at 40 °C. Finally, the solid material was collected and ground into a fine powder for use. The material was characterized by scanning electron microscopy, X-ray diffraction, half-cell cyclic voltammogram, and GCPL (Figure S1). Similar method was used for NiHCFe synthesis, with $Cu(NO_3)_2$ replaced by $Ni(NO_3)_2$ (Strem Chemicals).

2.2 Electrode preparation.

To prepare the CuHCFe/NiHCFe electrode, a mixture of 80 wt% CuHCFe/NiHCFe powder, 15 wt% carbon black, and 5 wt% polyvinylidene fluoride (PVDF) was hand-ground, with N-methyl-2-pyrrolidinone (NMP) added as solvent to form a slurry. Then, the slurry was dropped

onto carbon cloth (Fuel Cell Earth) and dried in a vacuum oven for 12 h at 40 °C. The mass loading of the CuHCFe electrode was approximately 5 mg cm^{-2} on an area of around 0.25 cm^2. The Ag electrode was prepared by mixing 80% silver powder (Sigma-Aldrich), 10 wt% carbon black, and 10 wt% PVDF into NMP solvent, dropped onto carbon cloth and dried in a vacuum oven for 12 h at 40 °C. The mass loading of the Ag electrode was approximately 8 mg cm^{-2} on an area of around 0.5 cm^2. The activated carbon electrode was prepared following the same procedure, with a mixture of 90 wt% activated charcoal and 10 wt% PVDF into NMP solvent, dropped onto a carbon cloth current collector with excessive mass loading and dried in a vacuum oven for 12 h at 40 °C. For the Cu electrode, Cu foil (thickness of ~10 µm) with an area of around 2 cm^2 was used after cleaning with isopropyl alcohol.

2.3 Cell fabrication and electrochemical characterization:

The continuous TREC system was mainly demonstrated in a two-electrode side-by-side pouch cell configuration (Figure S2a), with the CuHCFe electrode as the working electrode, the Cu electrode as the counter and reference electrodes, and a mixture of 0.5 M $RbNO_3$ and 0.2 M $Cu(NO_3)_2$ (pH of ~2 realized by adding nitric acid) as the electrolyte. Filter paper (Whatman) was placed between and under the electrodes for absorbing the electrolyte. The pouch cell was electrochemically characterized by GCPL (Figure S3), galvanostatic intermittent titration (Figure S4), and electrochemical impedance spectroscopy (Figure S5). The thermal stability of the cells was also examined (Figure S8).

The system was electrochemically tested in a three-electrode flooded beaker cell (Figure S2b), with CuHCFe serving as the working electrode and activated carbon as the counter electrode for half-cell tests and Cu electrode for full-cell tests, and Ag/AgCl in 4 M KCl solution as the reference electrode. The temperature coefficients of the CuHCFe cathode and Cu anode were tested in a full cell with a mixed electrolyte of 0.5 M $RbNO_3$ and 0.2 M $Cu(NO_3)_2$ (pH of ~2 by adding nitric acid).

A second system with the NiHCFe electrode as the working electrode, the Ag electrode as the counter electrode, and 1 M KCl as the electrolyte was tested in a similar way.

2.4 Lab-scale test bench design.

To control the applied temperature, a homebuilt setup was used (Figure S7). In brief, two circulators were used (Julabo Dyneo DD300F) to provide hot and cold fluids. Two valve clusters with normally closed motorized valves (Ymer Technology) were used to switch between hot and cold fluids. A timer was connected to control the switching frequency. The

pouch cell was placed in between the copper blocks and a K-type thermocouple was attached to the surface of each pouch cell. Data acquisition and operation control were realized using a potentiostat (VMP3, Biologic). The test apparatus allows rapid heat transfer between heat sources/sinks and the pouch cells (Figure S8, S16, S17, and S18), making temperature alternation nearly instantaneous.

3. Results and Discussion

3.1 Working principle of continuous TREC

To achieve continuous TREC operation, a straightforward working principle using two identical electrochemical cells compatible with various materials is proposed. In this demonstration, a copper hexacyanoferrate (CuHCFe) cathode and Cu/Cu^{2+} anode in a hybrid aqueous electrolyte are used in the identical cells (Figure 1a). The materials are selected due to the advantages of relatively large thermopower, notably small hysteresis, and cost-effectiveness thanks to its membrane-free characteristics. The redox reaction of each electrode is shown in Note S1 of the Supporting Information. The two cells experience four processes during each cycle: temperature alternation, discharging, temperature alternation, and discharging in the reverse direction (Figure 1b). When the two cells are in equilibrium and both anodes are electrically shorted (Step 0), the voltage difference between the cathodes of each cell is zero ($\Delta E = E_1 - E_2 = 0$). When the temperatures of the two cells are varied in Step 1, the potential of each cathode becomes different, leading to voltage output between the cathodes. For example, one cell (Cell 1) is heated to a given temperature (T_h) while the other (Cell 2) is cooled to a lower temperature (T_c). Assuming negative temperature coefficients of the cells, Cell 1 has a lower potential than Cell 2, and the open-circuit voltage (OCV) between the cells is negative ($\Delta E = E_1 - E_2 < 0$). When an electrical load is connected between the cathodes in Step 2, current flows spontaneously from Cell 2 to Cell 1 until the two cells achieve pseudo-equilibrium. In Step 3, the cells are disconnected from the load, and the temperatures are alternated by cooling Cell 1 to T_c while heating Cell 2 to T_h. The OCV between the cells then become positive ($\Delta E = E_1 - E_2 > 0$). When the electrical load is connected again in Step 4, current flows spontaneously from Cell 1 to Cell 2 until the two cells regain equilibrium. Thereafter, a new cycle starts in which these four steps are repeated.

To evaluate the performance of this continuous TREC system, we used two measuring approaches. The first approach, hereinafter referred to as the constant current mode, is electrochemical characterization by maintaining a constant current during discharging, as in galvanostatic cycling with potential limitation (GCPL). This mode is the conventional method

of testing electrochemical cells with well-defined conditions. The second approach, hereinafter referred to as the constant resistance mode, is output characterization by connecting an external resistance during discharging. This mode is a more practical demonstration of energy harvesting in that the system directly supplies electricity to external devices. Figure 1c (current vs. time (upper panel) and voltage vs. capacity (lower panel)) shows the expected output of the constant current mode. In Steps 2 and 4, constant currents with the same magnitude but opposite signs are applied to complete the discharging, whereas in Steps 1 and 3, no current is applied, and only the OCV is measured. Because both Steps 2 and 4 are discharging processes, the area of the loop curve in the voltage plot represents the net work harvested during the thermal energy conversion. Figure 1d depicts the constant resistance mode. The upper panel presents the external resistance load control over time under constant resistance. The resulting voltage and current output responses are shown in the middle and bottom panels, respectively. During the temperature alternation in Steps 1 and 3, the cells are regenerated, during which time the voltage output gradually increases and becomes saturated. When the external resistor is connected in Steps 2 and 4, the system forms a closed circuit, and the cells supply power to the external resistor; therefore, the cells gradually discharge until the voltage difference decays to zero. Correspondingly, the current initially surges to its peak and then gradually decreases to zero. Due to the temperature alternation, the voltage and the current outputs show alternating characteristics (i.e., the same variations but with opposite signs in each discharging process) during each cycle. Provided the temperature alternation is realized instantly, the proposed TREC system can generate a continuous low-voltage alternating current without support of an external device, thereby improving the practicability of TREC systems.

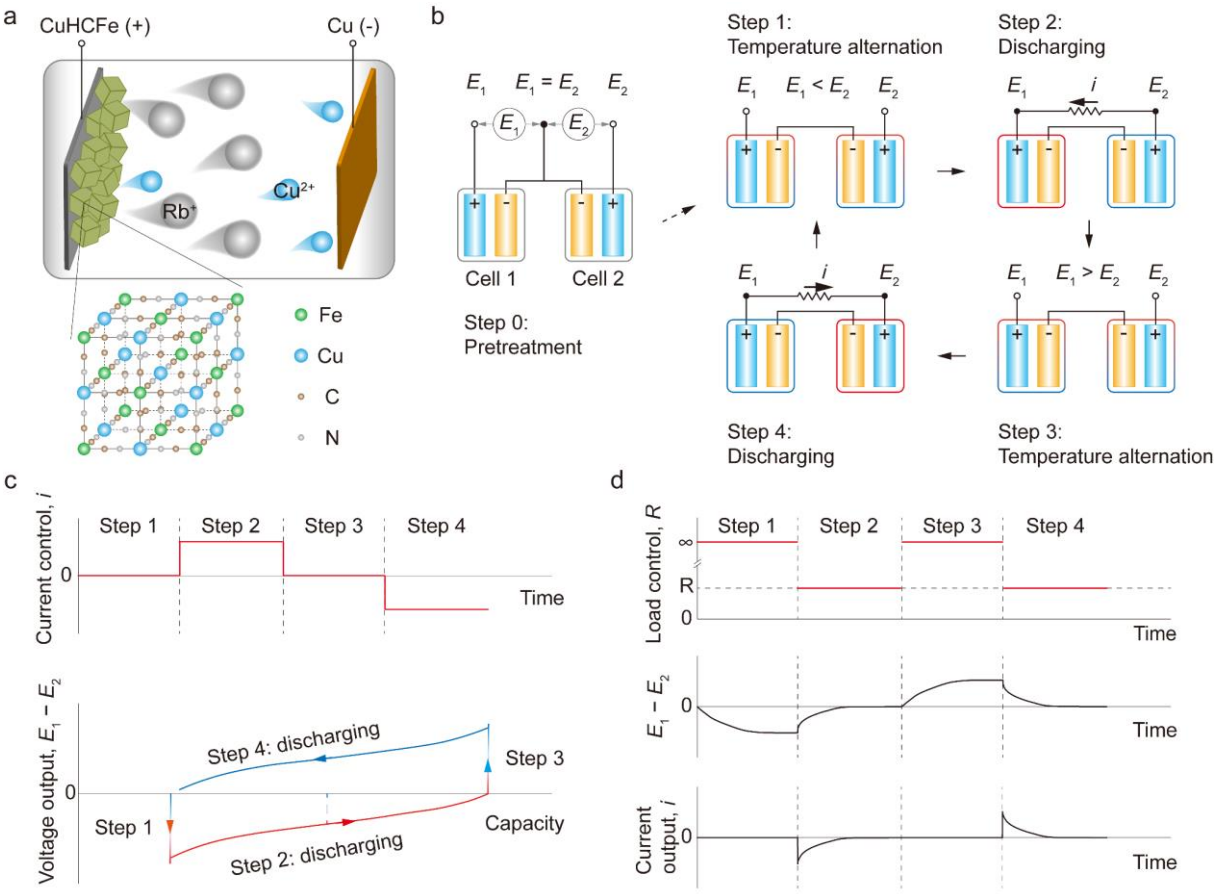

Figure 1. Working principle of continuous TREC for thermal energy harvesting. a) Investigated full cell configuration with a CuHCFe cathode and a Cu/Cu^{2+} anode in a hybrid electrolyte of 0.5 M $RbNO_3$ and 0.2 M $Cu(NO_3)_2$. b) Schematics of the cycling processes: Step 0, pretreatment of the cells to the equilibrium state; Step 1, temperature alternation of the cells; Step 2, spontaneous discharging; Step 3, temperature alternation of the cells; Step 4, spontaneous discharging in the opposite direction. c) Constant current mode of continuous TREC. Current control over time (upper panel) and the corresponding voltage−capacity (bottom panel) plots are given. The area of the loop curve in the voltage plot represents the net work harvested during the thermal energy conversion. d) Constant resistance mode of continuous TREC. Load control over time (upper panel) and the resulting voltage (middle panel) and current output responses (bottom panel) are presented.

3.2 Electrochemical characterization of continuous TREC

The performance of the as-assembled side-by-side pouch cell (Figure S2a, Supporting Information) was characterized by GCPL with CuHCFe as the cathode and Cu foil as the anode in a hybrid electrolyte containing 0.5 M $RbNO_3$ and 0.2 M $Cu(NO_3)_2$. As shown in Figure S3 of the Supporting Information, the cell was cycled between 0.6 and 1.0 V at a current density

of 60 mA g^{-1} (1 C) for the mass of CuHCFe. One plateau was observed clearly at around 0.78 V in the hybrid electrolyte. The corresponding discharge capacity was 56.61 mAh g^{-1} in the first cycle. After charging/discharging for 97 cycles at 1 C, the specific capacity was 56.66 mAh g^{-1}, and the average coulombic efficiency was 99.58%. These results demonstrate the stable electrochemical performance of the cell. Two identical pouch cells were assembled for further investigation; their GCPL curves at a cycling rate of 1 C are shown in Figure 2a. The specific discharge capacity and the coulombic efficiencies were 58.13 and 60.17 mAh g^{-1} and 98.91% and 98.78% for Cells 1 and 2, respectively.

The temperature coefficient (α) is an important factor determining the voltage output in a TREC for a given temperature difference. The α of each electrode was measured in a three-electrode flooded beaker cell with an Ag/AgCl reference electrode (Figure S2b, Supporting Information). The open-circuit potential was recorded for each electrode when the temperature was increased stepwise from 10 to 40 °C and then decreased to 10 °C in 10 °C intervals (Figure 2b). The voltage changes of each electrode exhibit a linear trend with temperature variation, indicating a constant α for each electrode within the investigated temperature window (Figure 2c). The calculated α for the CuHCFe electrode (50% state of charge (SOC)), Cu/Cu^{2+} electrode, and full cell are −1.097, 0.659, and −1.756 mV K^{-1}, respectively. The temperature coefficient of the full cell in the pouch cell configuration used in the TREC tests (including α vs SOC; Figure S6, Supporting Information) was measured and found to show nearly the same values.

To demonstrate the performance of the continuous TREC, the first approach is to run a system of two identical cells in the constant current mode. Figure 2d shows the voltages of each cell over one continuous TREC cycle when the temperature is alternated between 10 and 50 °C at a constant current density of 11.96 mA g^{-1} (0.2 C) for the mass of CuHCFe in both cells (i.e., all current and energy densities are based on the total mass of CuHCFe in both cells). The corresponding voltage output of the system over one continuous TREC cycle is given in Figure 2e. In Step 1, as Cell 1 is heated from 10 to 50 °C, its OCV decreases from 0.763 to 0.697 V, while as Cell 2 is cooled from 50 to 10 °C, its OCV increases from 0.763 to 0.826 V. Correspondingly, the voltage output of the system increases from 0 to 0.129 V. Then, Cell 1 is charged at 50 °C while Cell 2 is discharged at 10 °C for 214 min to gradually arrive at the same voltage when the two CuHCFe electrodes are electrically connected in Step 2. An additional 31-min shorting is implemented in this step to achieve equilibrium of the two electrodes. In Step 3, as Cell 1 is cooled from 50 to 10 °C, its OCV increases from 0.762 to 0.827 V, while as Cell 2 is heated from 10 to 50 °C, its OCV decreases from 0.762 to 0.694 V. Meanwhile, the voltage output of the system increases from 0 to 0.133 V. Finally, Cell 1 is discharged at 10 °C

while Cell 2 is charged at 50 °C to gradually arrive at the same voltage when the two CuHCFe electrodes are electrically connected in Step 4. Similarly, an additional shorting is implemented in this step to achieve equilibrium of the two electrodes. At the end of Step 4, the final voltage of each cell is the same as the initial voltage in Step 1, meaning that as one cycle finishes, the next cycle starts with temperature alternation.

The voltage plots of the two cells as a function of specific capacity are shown in Figure 2f. Due to the negative temperature coefficients, the charging voltage curves at high temperature are below the discharging voltage curves at low temperature for both cells, indicating energy gain instead of energy loss during the TREC cycle. The plot of output voltage as a function of specific capacity is presented in Figure 2g. Both discharging processes are observed in Steps 2 and 4. The slight voltage spikes at the beginning of each process are caused by the overpotential and internal resistance of the cells. At the end of the second discharging process, the curve does not form a perfect closed loop for two reasons. First, because the Coulombic efficiencies of the two cells are less than 100%, electric charge losses are inevitable (Figure 2a). Second, after arriving at the same voltage at the end of the discharging process at a constant current density, the cells discharge further at a gradually decayed current density to realize equilibrium. The curves for these additional shorting processes are not presented here because they do not contribute to power generation at a voltage output of zero. The area of the loop is the net work generated from low-grade energy harvesting. The calculated energy density of the demonstrated continuous TREC is 9.69 J g^{-1}; the resulting energy conversion efficiency is 1.76% without heat recuperation, corresponding to 14.19% of the Carnot efficiency. The energy conversion efficiency can be improved to 3.08% and 5.60% if heat recuperation efficiencies of 50% and 80% are realized, corresponding to 24.84% and 45.21% of the Carnot efficiency, respectively (Note S2 and Table S1, Supporting Information).

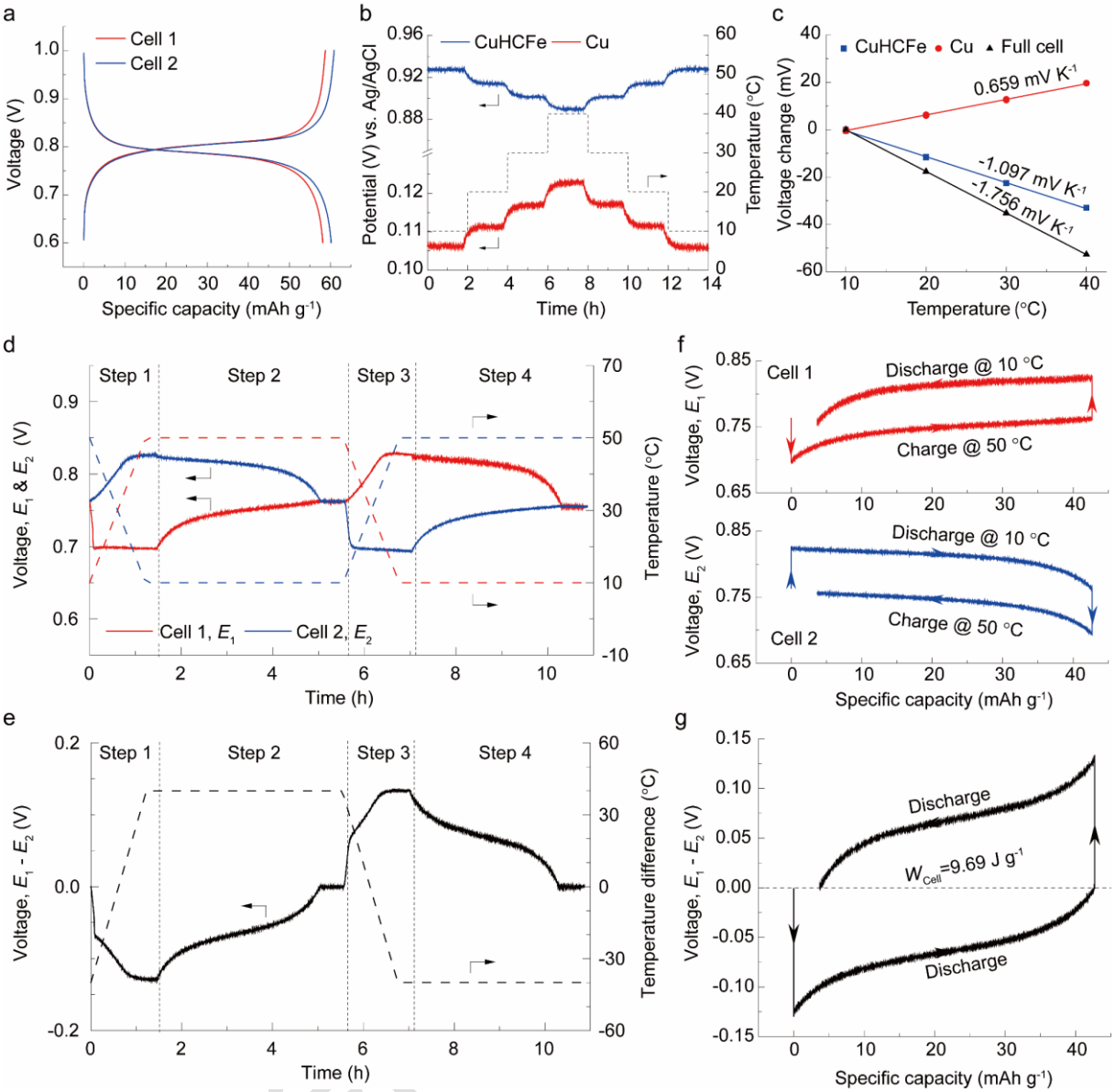

Figure 2. Electrochemical characterization of continuous TREC in constant current mode. a) Galvanostatic cycling with potential limitation (GCPL) curves of two identical pouch cells with CuHCFe cathode and Cu/Cu^{2+} anode. b) Open-circuit potential of the CuHCFe electrode (50% state of charge) and the Cu electrode when the temperature was increased stepwise from 10 to 40 °C and then decreased to 10 °C in 10 °C intervals. c) Voltage changes of the CuHCFe electrode, the Cu electrode, and the full cell compared with the initial voltage at 10 °C with the same conditions as in (b). The slopes of the linear fitting lines represent the temperature coefficients of electrodes and the full cell. d) Voltages of each cell over one continuous TREC cycle when the temperature is alternated between 10 and 50 °C and the discharging is at a constant current density of 11.96 mA g^{-1} (0.2 C). The temperature variations are shown by the dash lines (red for Cell 1, blue for Cell 2), which are artificially superimposed for clarity. e) Output voltage of the system over one continuous TREC cycle with the same condition as in

(d), defined as E_1 of Cell 1 minus E_2 of Cell 2 in this paper. The temperature difference is shown by the dash line, defined as the temperature of Cell 1 minus the temperature of Cell 2. f,g) Voltage plots of each cell f) and the system g) as a function of specific capacity of CuHCFe over one continuous TREC cycle with the same conditions as in (d).

To further explore the capabilities of the proposed continuous TREC system in low-grade energy harvesting, we tested the system at various current densities and temperature differences. Figure 3a presents voltage as a function of specific capacity (based on the mass of CuHCFe in Cell 1) during one cycle at different C rates of 0.1, 0.2, 0.5, and 1 C when the temperature is alternated between 10 and 50 °C. The utilized capacity tends to increase at low current densities due to the reduction in the losses caused by the overpotential and internal resistance at the beginning of each discharging process. However, this tendency changes when the current density decreases to 0.1 C because the Coulombic efficiency of CuHCFe decreases due to self-discharging. The absolute energy conversion efficiencies, without considering heat recuperation effects, are 1.80%, 1.76%, 1.56%, and 1.24% at 0.1, 0.2, 0.5, and 1 C, respectively, which correspond to relative efficiencies of 14.51%, 14.19%, 12.59%, and 10.03%, respectively. If 50% heat recuperation efficiency is achieved, then the respective expected absolute energy conversion efficiencies are 3.14%, 3.08%, 2.73%, and 2.19%; these efficiencies can be further increased to 5.68%, 5.60%, 4.97%, and 4.04% at 80% heat recuperation efficiency, corresponding to relative efficiencies of 45.86%, 45.21%, 40.19%, and 32.67%, respectively (Figure 3b and Table S2, Supporting Information). The energy densities of the TREC between 10 and 50 °C at 0.1, 0.2, 0.5, and 1 C are 7.22, 9.69, 8.35, and 6.07 J g^{-1}, respectively (Figure 3c). These results suggest the demonstrated charging-free continuous TREC system has good rate capability and high energy conversion efficiency even at 1 C.

Figure 3d depicts voltage as a function of specific capacity during one cycle at various temperature differences (ΔT) of 10, 20, 30, and 40 °C at a constant current density of 0.2 C and a fixed low temperature of 10 °C. The corresponding calculated absolute energy conversion efficiencies, without considering heat recuperation effects, are 0.68%, 1.48%, 1.59%, and 1.76%, corresponding to relative efficiencies of 19.89%, 22.46%, 16.62%, and 14.19%, respectively (Figure 3e); the resulting energy densities are 0.58, 3.71, 6.32, and 9.69 J g^{-1}, respectively (Figure 3f). Considering heat utilization in the two cells, the absolute energy conversion efficiencies can be improved to 1.01%, 2.41%, 2.73%, and 3.08% at 50% heat recuperation efficiency and to 1.44%, 3.87%, 4.77%, and 5.60% at 80% heat recuperation efficiency, respectively. The corresponding relative efficiencies are 29.67%, 36.56%, 28.49%,

and 24.84% at 50% heat recuperation efficiency and 42.08%, 58.64%, 49.84%, and 45.21% at 80% heat recuperation efficiency (Figure 3e and Table S1, Supporting Information). Furthermore, the TREC system has great potential for energy harvesting at around room temperature. As shown in Figure 3d, 3e, and 3f, when the temperature is alternated between 25 and 35 °C, the system achieves energy efficiencies of 0.98% (absolute) and 30.08% (relative) without heat recuperation (Figure 3e). With 80% heat recuperation efficiency, the efficiency can be substantially improved to 2.06%, corresponding to 63.35% of the Carnot efficiency (Figure 3e and Table S1, Supporting Information). The calculated energy density is 0.94 J g^{-1} (Figure 3f). The performance in this temperature range is better than that when the system is cycled between 10 and 20 °C, owing to faster kinetics at higher temperatures. These results demonstrate that the continuous TREC system is promising for low-grade energy harvesting even at a narrow temperature difference of 10 °C.

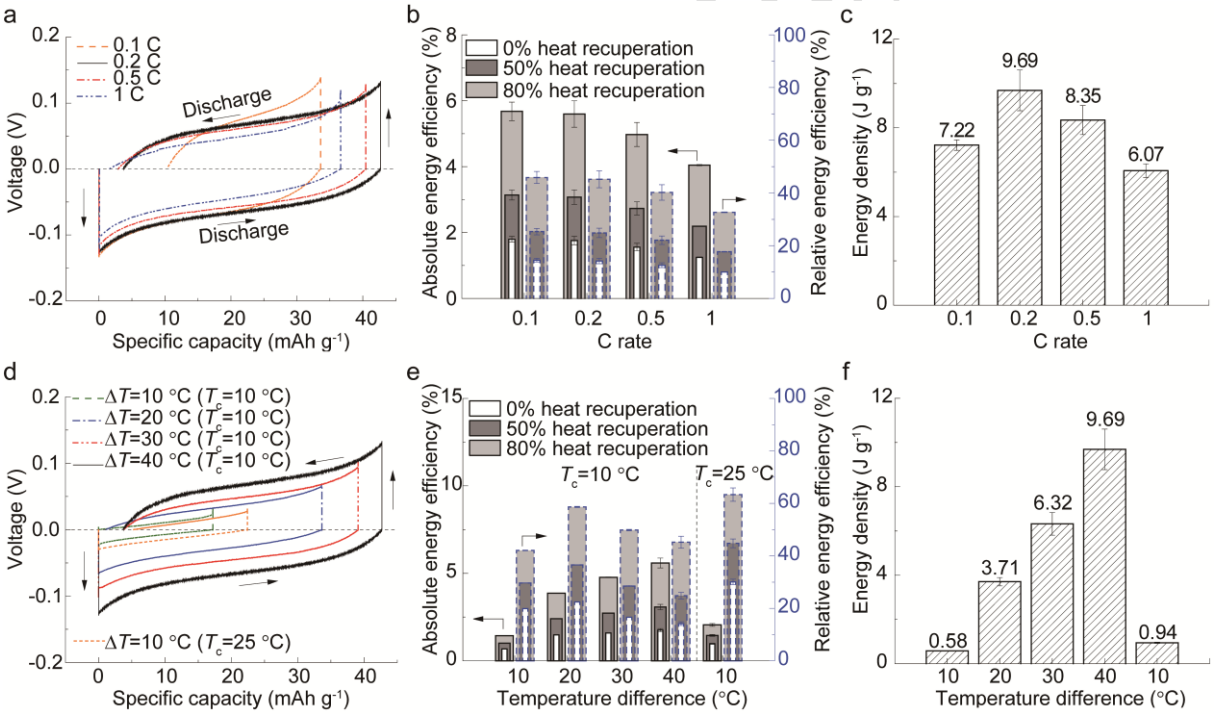

Figure 3. Performance of continuous TREC at various current densities and temperature differences. a) Voltage as a function of specific capacity during one cycle at different C rates of 0.1, 0.2, 0.5, and 1 C when the temperature is alternated between 10 and 50 °C. b) Comparison of the calculated absolute and relative energy conversion efficiencies at different heat recuperation efficiencies with the same conditions as in (a). c) Measured energy density without considering heat recuperation effects with the same conditions as in (a). d) Voltage as a function of specific capacity during one cycle at various temperature differences of 10, 20, 30, and 40 °C at a constant current density of 0.2 C. e) Comparison of the calculated absolute

and relative energy conversion efficiencies at different heat recuperation efficiencies with the same conditions as in (d). f) Measured energy density without considering heat recuperation effects with the same conditions as in (d). Error bars represent the standard deviations.

3.3 Output performance of continuous TREC in constant resistance mode

To quantify the output performance of the continuous TREC system for practical power supply to external systems, it is essential to investigate the voltage and current outputs as a function of the external load resistance, as shown in Figure 4 (the test set-up and circuit details are shown in Figure S7, Supporting Information). Figure 4a–d shows the results of the continuous TREC system comprising a single pair of cells in the constant resistance mode when the temperature is periodically alternated between 10 and 50 °C (the test procedure is detailed in Note S3, Supporting Information). When the cell is heated, the OCV of the cell gradually decreases and eventually saturates at high temperature, and vice versa (Figure 4a). The corresponding voltage output of the system is displayed in Figure 4b. Even after periodic repetition, the absolute saturated voltage remains stable and constant. The cells were tested starting at 50% SOC and shorted without external resistance (0 Ω) to achieve equilibrium in the first 2.4 h. Later, for each temperature alternation, the voltage output plateaus at around 0.13 V, with cell voltages of around 0.70 V at 50 °C and around 0.83 V at 10 °C (Table S3, Supporting Information). Then, the cells were subjected to periodic temperature alternation and discharging with external resistance. Repeatability was characterized under constant resistance (Figure S9, Supporting Information). Figure 4c presents the short-circuit current responses when the external resistance was varied sequentially from 0 to 50, 100, 200, 300, and 400 Ω. The responses shown are consistent at each of these external resistances (Figure 4d): an initial upsurge to its peak, followed by a gradual reduction to almost zero (less than 1 μA) to reach a new equilibrium. The current alternates from positive to negative, while the absolute peak current decreases with increase in the load. The peak current density reaches 0.35 A g^{-1} without external resistance and decreases from 0.26 to 0.12 A g^{-1} as the external resistance is increased from 50 to 400 Ω (Figure 4d and Table S3, Supporting Information). The corresponding specific peak power shows a parabolic variation trend as a function of external resistance (Figure 4e). The specific peak power is the maximum (estimated to be 12.05 mW g^{-1}) at an external resistance of approximately 260 Ω. The energy delivered to the external resistance was derived for each discharging process; the output energy density was found to vary similar to the specific peak power, first growing and then decreasing with increasing external resistance (Figure 4f). The estimated maximum output energy density is 1.94 J g^{-1} when the system is operated between

10 and 50 °C (Note S4, Supporting Information). The power density is calculated as 2.02 mW g^{-1}, which is quite close to the maximum of 2.76 mW g^{-1} (Note S5, Supporting Information). The corresponding output efficiency without considering heat recuperation effects is 0.85%, nearly half the maximum efficiency of 1.80% (Table S2, Supporting Information).

Similar tests were conducted to examine the output performance of the continuous TREC at different temperature differences (Figure 4d–f). The short-circuit current density decreases with the narrowing of the temperature difference because of a reduction in the OCV output of the system (Figure 4d, Table S4–7, Supporting Information). The specific peak power maintains its parabolic variation with a change in the external resistance; however, the maximum peak power substantially decreases as the temperature difference is narrowed because power is proportional to the square of the current (Figure 4e). Similarly, the optimal output energy density decreases with a narrowing temperature difference (Figure 4f). The estimated peak power values are 5.62 mW g^{-1} (at an external resistance of 290 Ω) and 1.71 mW g^{-1} (at 460 Ω), and the achieved maximum energy densities are 1.66 J g^{-1} (at 400 Ω) and 1.01 J g^{-1} (at 600 Ω) when the temperature difference is lowered to 30 and 20 °C, respectively (Table S4 and Table S5, Supporting Information). These results indicate that while a larger temperature difference results in a better output performance because of a larger voltage output, reasonable performance can also be achieved with the proposed system at an ultralow temperature difference of 10 °C. The peak current density, maximum specific peak power, and the energy density remain largely unchanged for temperature alternations between 10 and 20 °C and between 25 and 35 °C (Figure 4d–f). The average estimated maximum specific peak power is 0.53 mW g^{-1} at an external resistance of 360 Ω, and the achieved maximum energy density is 0.26 J g^{-1} at around 380 Ω (Table S6 and Table S7, Supporting Information).

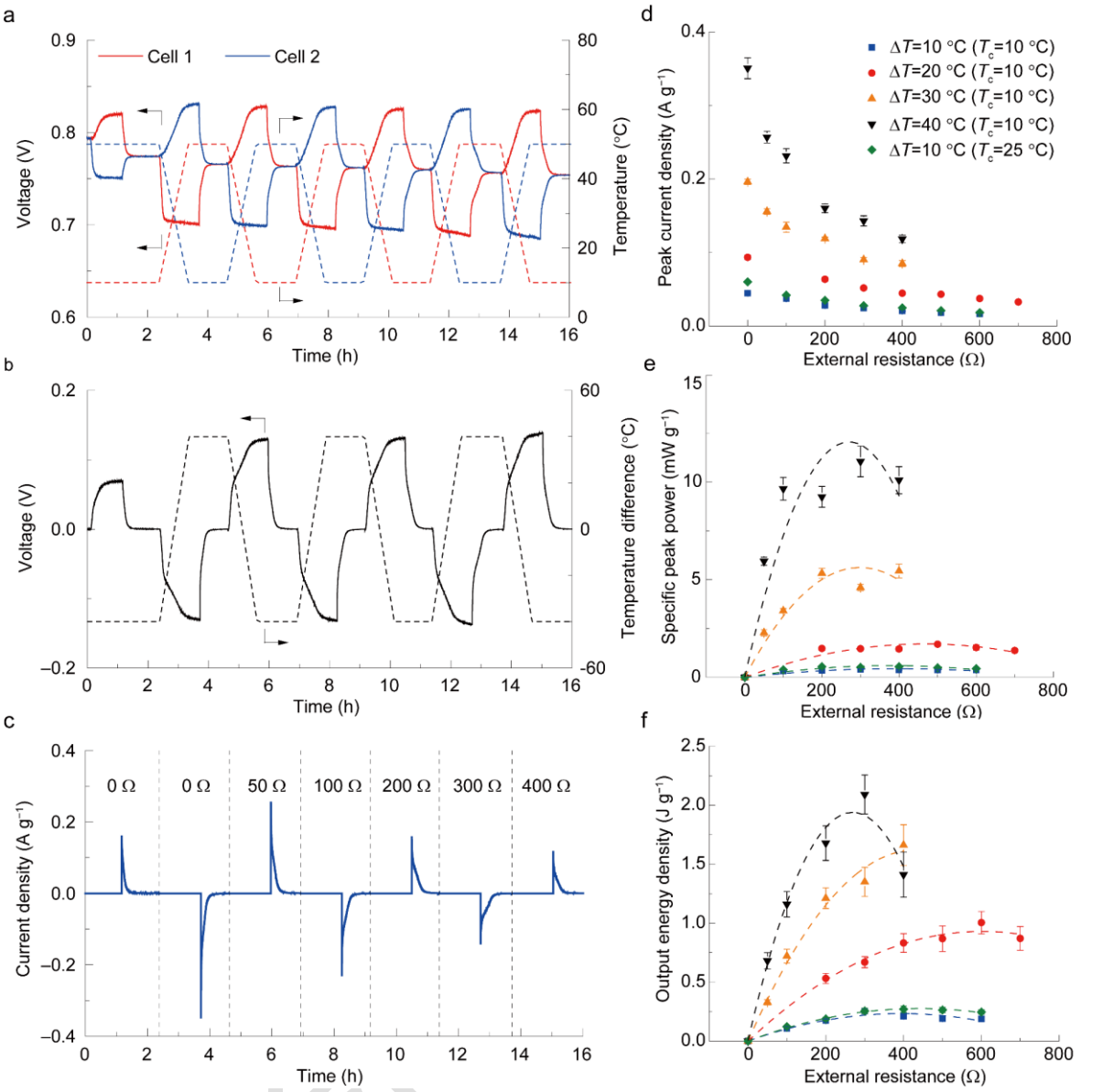

Figure 4. Output performance of continuous TREC with a single pair of cells in constant resistance mode. a) Voltage responses of the two cells under periodic temperature alternation between 10 and 50 °C. The corresponding temperature profiles of each cell are shown by the dash lines. The cells were tested starting at 50% SOC thus the cells show lower voltages during the first temperature alternation, which was excluded in performance quantification. b) Voltage output of the system along with the artificially defined temperature difference of the system with the same conditions as in (a). c) Corresponding short-circuit current responses when the external load resistance was varied sequentially from 0 to 50, 100, 200, 300, and 400 Ω with the same conditions as in (a). Specific current density is used to eliminate the influences of total mass of the active materials. d–f) Main outputs as a function of external load resistance at different temperature differences. Average values of at least 3 replicates are indicated with error bars representing the standard deviations: d) absolute peak current density; e) specific peak

power delivered to the external resistance (scatters are the results calculated by the measured data, dash lines are the fitting curves); and f) output energy density generated at the external resistance (scatters are the results calculated by the measured data, dash lines are the fitting curves).

3.4 Long-term cycling of continuous TREC

The cycling performance of the continuous TREC for temperature alternation between 10 and 50 °C is shown in Figure 5. The tests were conducted with only one pair of cells, which were initially pretreated to 40% and 60% SOC, respectively. A near-optimal external resistance of 300 Ω was connected to evaluate the output performance. The absolute output efficiency is 1.17% in the first cycle, corresponding to 9.49% of the Carnot efficiency at 50% heat recuperation efficiency. The system maintains more than 80% of its efficiency after 97 cycles (Figure 5a), beyond which the efficiency decreases significantly due to the voltage shifting of each cell caused by hysteresis and internal resistance. After 114 cycles, the total charge decreases to less than 36.8% (defined as a decay constant for judging the shifting of the cell voltages in this paper) of the initial charge (0.055 C) (Figure 5b). On refreshing, the system recovers well, with an absolute efficiency of 1.07% in the first cycle (Figure 5a) and completion of 120 cycles before severe shifting is observable (Figure 5b). At 80% heat recuperation efficiency, the expected absolute output efficiency is 2.16% (Figure S12a, Supporting Information), corresponding to 17.46% of the Carnot efficiency (Figure S12b, Supporting Information). Even after two long-term cycling tests (totaling 234 cycles), both cells remain rather healthy, with almost no decay in capacity and coulombic efficiency relative to the pristine cells (Figure S12c–d, Supporting Information). Figure 5c compares the current responses for several typical cycles during long-term cycling. Before voltage shifting occurs, there is no significant change in the overall shape, either in the first long-term cycling test or the post-refreshment tests (i.e., in the 1st, 55th, 78th, 115th, and 174th cycles). When voltage shifting is observed, the current response curves are much steeper at the beginning of each discharging process, which is caused by the large hysteresis and rapidly growing cell voltage when the cell voltage is located outside the plateau (i.e., in the 97th, 114th, and 234th cycles). Such voltage shifting and cell refreshment can be minimized by decreasing the cell hysteresis and internal resistance and through effective cell lifecycle management (Note S6, Supporting Information). The long-term cycling performance of the proposed system with a larger utilized capacity was also studied. By starting the process from 30% SOC for Cell 1 and 70% SOC for Cell 2, the output efficiency is improved to 2.01% in the first cycle at 50% heat recuperation efficiency,

corresponding to 16.01% of the Carnot efficiency. The system has the potential to realize 3.12% absolute efficiency and 25.17% relative efficiency at 80% heat recuperation efficiency when operated between 10 and 50 °C (Figure S13, Supporting Information).

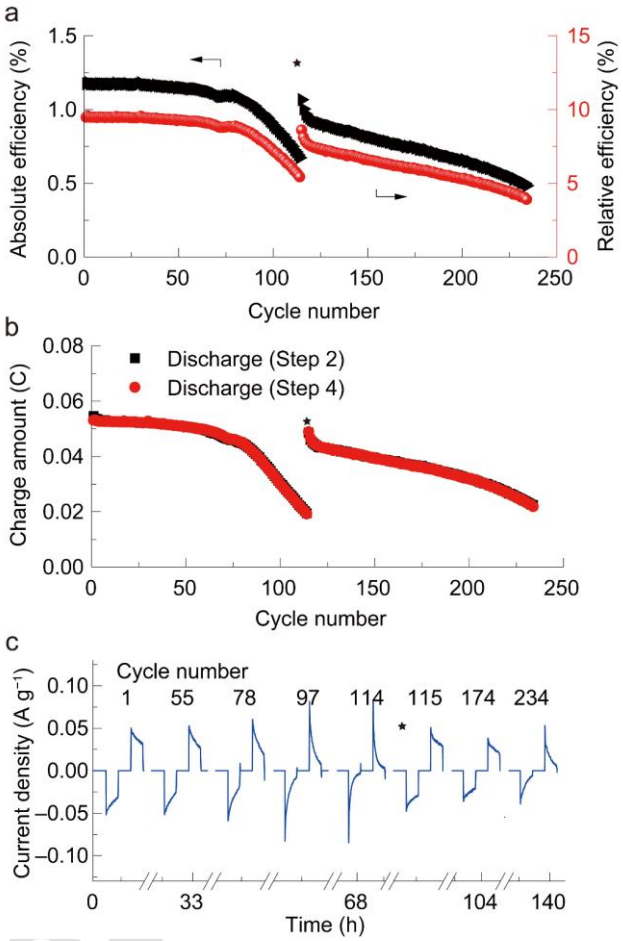

Figure 5. Cycling performance of continuous TREC with a single pair of cells when the temperature is alternated between 10 and 50 °C in constant resistance (300 Ω) mode. a) Output efficiency at 50% heat recuperation efficiency. Dark triangle indicates the absolute efficiency. Red sphere represents the relative efficiency to the Carnot efficiency. The asterisk denotes the refreshment due to the voltage shifting caused by the overpotential and the internal resistance. b) The total charge during the discharging processes. The dark rectangles and red circles denote the total charge during the first half cycle (Step 2) and the second half cycle (Step 4), respectively. c) Short-circuit current responses in the 1st, 55th, 78th, 97th, 114th, 115th, 174th, and 234th cycles.

4. Discussion

We firstly discussed on the power density. Because the target application of the developed continuous TREC system is direct power supply to external systems, power density is an important factor affecting its practicability. We estimated the power density of the proposed continuous TREC in both the constant current and constant resistance modes. The estimated maximum power density is 2.76 mW g^{-1} for temperature alternation between 10 and 50 °C at a current density of 37.55 mA g^{-1} (Figure S10, Supporting Information), which is the highest power density reported thus far (Table S8 and Figure S14, Supporting Information). This improvement is due to the enlarged voltage gap between the two discharging processes in a cycle, which originates from the differences in the temperature and SOC of each cell. As analyzed in Note S5 of the Supporting Information, the power density depends on the total mass of the CuHCFe in both cells, the applied current density, and the voltage gap between the two discharging processes in each cycle. The maximum power density is achieved at the optimal current density. The power density can be further improved by exploring electrode materials with higher specific capacities and flat charge/discharge curves to enlarge the capacity range that can be utilized, and those with larger temperature coefficients to increase the voltage difference between two discharging processes, and by widening the temperature difference between the cells. Our results confirmed that the developed TREC system can successfully direct power supply to external devices, with a maximum power density (2 mW g^{-1}) achieved at a matched resistance (Note S5, Supporting Information). The results obtained in the two modes are consistent, evidencing the practicability of the continuous TREC system for low-grade thermal energy harvesting.

Then, we gave evidence on the freedom of material selection. Comparing with the charging-free TREC proposed in [34], which has strict constraints on materials, our continuous operation scheme is extremely flexible given its independence of the electrode materials. To prove this, we demonstrated another continuous TREC system, with nickel hexacyanoferrate (NiHCFe) as the working electrode, silver (Ag) as the counter electrode, and 1 M KCl as the electrolyte. Results were presented in Figure S16 for the operation in constant current mode, Figure S17 for the operation in constant resistance mode, and Figure S18 for the preliminary demonstration on cycling performance (Supporting Information). All are tested when the temperature is periodically alternated between 10 and 50 °C. The calculated energy density is 1.99 J g^{-1} (Figure S16, Supporting Information); the resulting energy conversion efficiency is 1.56% without heat recuperation, which can be enhanced to 2.71% with 50% heat recuperation efficiency. When the cells are connected to the external resistance, the specific peak power reaches its peak (4.33 mW g^{-1}) at 300 Ω (Figure S17, Supporting Information). The system also

maintained good cycling stability with no decay observed for the studied 11 cycles (Figure S18, Supporting Information).

Thirdly, we compared the performance with literatures. Detailed discussions for a relatively fair comparison were given in Table S10 and Note S7 (Supporting Information). Figure 6 presents the comparison results with technologies including TREC [22,27,30,33], TGC [12,37−41], thermo-osmotic energy conversion system (TOEC) [42], direct thermal charging cell (DTCC) [43], thermally regenerative battery (TRB) [44−53], pressure-retarded osmosis (PRO) [54], reverse electrodialysis (RED) [54,55], and thermally regenerative flow battery based on copper-acetonitrile complexation (CuACN) [56]. It clearly shows that the TREC is extremely promising due to the highest efficiency among these technologies, which greatly outperforms others from the perspective of relative efficiency to the Carnot efficiency, although the areal power density needs to be improved. With heat recuperation considered in TREC, the efficiency can be further improved significantly. Besides, our system is membrane-free, which further highlights the practicability in real applications thanks to the cost reduction.

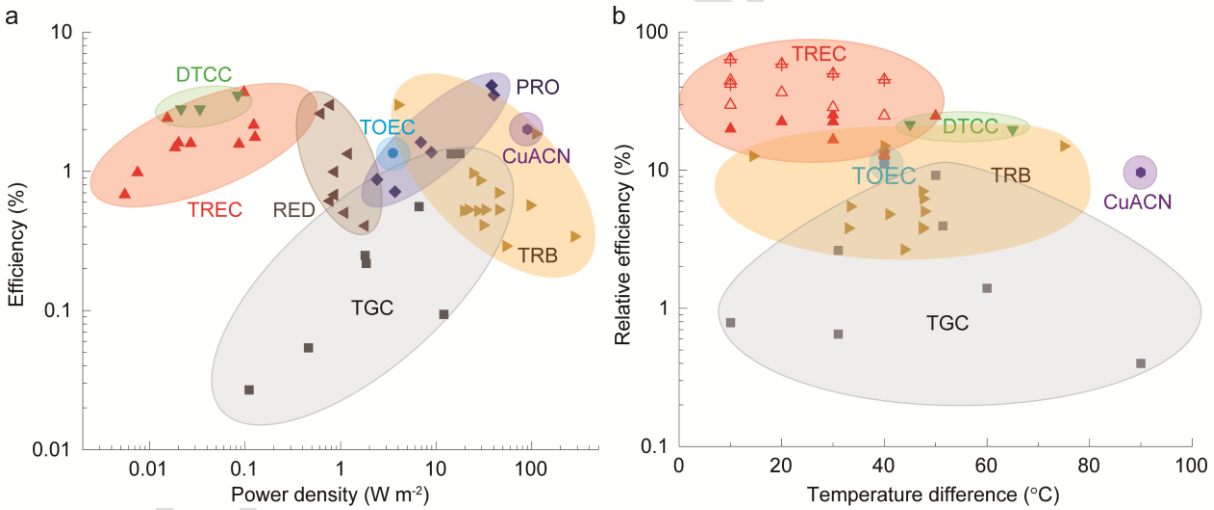

Figure 6. Comparison with literatures. a) Efficiency versus areal power density. b) Efficiency relative to the Carnot efficiency versus temperature difference. Hollow red triangle means 50% heat recuperation considered in TREC, while red triangle with cross means 80% heat recuperation considered in TREC. Numerical values are summarized in Table S10 and discussed in detail in Note S7 (Supporting Information).

Finally, we briefly addressed the potential application scenarios with the proposed system. With the pouch cell configuration and flow regulation circuits, the temperature alternation can be realized nearly instantaneously, as shown in Figure S8, S16, S17, and S18. It is worth pointing

out that we intentionally slowed down the temperature alternation processes for better illustration of the four-step working principles as shown in Figure 2 and 4, which should not be regarded as a break of the continuity of electricity generation. The duration for temperature alternation depends on the heat transfer rate between the heat source/sink and the cells. Hence, the system is applicable for industrial waste heat harvesting. For those heat sources in the form of liquid (e.g., wastewater), it can be directly circulated to transfer heat to the electrochemical cells. For gaseous waste heat carriers (e.g., exhaust gases), it is suggested to adopt a heat exchanger to transfer heat to liquid fluids first before interacting with the electrochemical cells. While for the cooling medium, room-temperature water can be directly used. Actually, any two waste carriers at different temperatures in any place can drive the proposed system. Only a flow management circuit, consisting of the valve sets and piping, is required to guide the temperatures delivered to the cells.

5. Conclusion

In summary, a continuous thermally regenerative electrochemical system is proposed for direct electricity generation from low-grade heat and demonstrated with a CuHCFe cathode, a Cu/Cu^{2+} anode, and a Rb/Cu ion hybrid aqueous electrolyte. The use of identical electrochemical cells operated under periodic temperature alternation effectively eliminated the additional electricity requirement for cell regeneration. The system shows an energy conversion efficiency of 1.76% (14.19% of the Carnot efficiency) when alternated between 10 and 50 °C without any heat recuperation, which can be improved to 5.60% (45.21% of the Carnot efficiency) at 80% heat recuperation efficiency. This large energy conversion efficiency is enabled by the freedom that the proposed system affords in selecting electrode materials with large temperature coefficients, without considering their electrochemical potential. When powering an external device, the maximum output performance is achieved at a matched resistance, and the output efficiency is halved (0.85% without heat recuperation). Furthermore, the system is feasible at various temperature differences, even at an ultralow temperature difference near room temperature. A cycle efficiency of 0.98% is achieved at a very low temperature difference of 10 °C (i.e., when operated between 25 and 35 °C) without any heat recuperation. In addition, the system exhibits good cycling performance, with almost no cell degradation after 234 cycles when cell refreshment is performed to compensate for voltage shifting. The developed continuous thermally regenerative electrochemical system is flexible, scalable, and cost-effective and can be applied to any material or cell configuration, advancing the practicability of such systems for direct low-grade thermal energy conversion.

Appendix A. Supporting Information

Supporting Information is available online at https://www.journals.elsevier.com/nano-energy.

Acknowledgements

This work was supported by Ministry of Education, Singapore under ref. no. MOE2019-T2-1-122.

Declaration of Competing Interests

The authors declare no conflict of interest. The authors declare that they have no known competing financial interests or personal relationships that could have appeared to influence the work reported in this paper.

References

[1] S. Chu, A. Majumdar, Opportunities and challenges for a sustainable energy future, Nature 488 (2012) 294-303.

[2] A. Thekdi, S. U. Nimbalkar, Industrial waste heat recovery - Potential applications, available technologies and crosscutting R&D opportunities, https://info.ornl.gov/sites/publications/files/Pub52987.pdf, accessed: 13th February 2021.

[3] E. Bell Lon, Cooling, heating, generating power, and recovering waste heat with thermoelectric systems, Science 321 (2008) 1457-1461.

[4] J. He, T. M. Tritt, Advances in thermoelectric materials research: Looking back and moving forward, Science 357 (2017) eaak9997.

[5] X. Li, B. Xu, H. Tian, G. Shu, Towards a novel holistic design of organic Rankine cycle (ORC) systems operating under heat source fluctuations and intermittency, Renew. Sustain. Energy Rev. 147 (2021) 111207.

[6] L.-D. Zhao, V. P. Dravid, M. G. Kanatzidis, The panoscopic approach to high performance thermoelectrics, Energy Environ. Sci. 7 (2014) 251-268.

[7] L.-D. Zhao, G. Tan, S. Hao, J. He, Y. Pei, H. Chi, H. Wang, S. Gong, H. Xu, V. P. Dravid, C. Uher, G. Jeffrey Snyder, C. Wolverton, M. G. Kanatzidis, Ultrahigh power factor and thermoelectric performance in hole-doped single-crystal SnSe, Science 351 (2016) 141-144.

[8] B. F. Tchanche, G. Lambrinos, A. Frangoudakis, G. Papadakis, Low-grade heat conversion into power using organic Rankine cycles – A review of various applications, Renew. Sustain. Energy Rev. 15 (2011) 3963-3979.

[9] X. Li, S. Lecompte, J. Van Nieuwenhuyse, K. Couvreur, H. Tian, G. Shu, M. De Paepe, C. N. Markides, Experimental investigation of an organic Rankine cycle with liquid-flooded expansion and R1233zd(E) as working fluid, Energy Convers. Manag. 234 (2021) 113894.

[10] T. I. Quickenden, Y. Mua, A review of power generation in aqueous thermogalvanic cells, J. Electrochem. Soc. 142 (1995) 3985.

[11] T. I. Quickenden, C. F. Vernon, Thermogalvanic conversion of heat to electricity, Sol. Energy 36 (1986) 63-72.

[12] J. Duan, G. Feng, B. Yu, J. Li, M. Chen, P. Yang, J. Feng, K. Liu, J. Zhou, Aqueous thermogalvanic cells with a high Seebeck coefficient for low-grade heat harvest, Nat. commun. 9 (2018) 1-8.

[13] E. H. B. Anari, M. Romano, W. X. Teh, J. J. Black, E. Jiang, J. Chen, T. Q. To, J. Panchompoo, L. Aldous, Substituted ferrocenes and iodine as synergistic thermoelectrochemical heat harvesting redox couples in ionic liquids, Chem. Commun. 52 (2016) 745-748.

[14] M. Li, M. Hong, M. Dargusch, J. Zou, Z. -G. Chen, High-efficiency thermocells driven by thermo-electrochemical processes, Trends in Chemistry 3 (2021) 561-574.

[15] T. Migita, N. Tachikawa, Y. Katayama, T. Miura, Thermoelectromotive force of some redox couples in an amide-type room-temperature ionic liquid, Electrochemistry 77 (2009) 639-641.

[16] L. Jin, G. W. Greene, D. R. MacFarlane, J. M. Pringle, Redox-Active Quasi-Solid-State Electrolytes for Thermal Energy Harvesting, ACS Energy Lett. 1 (2016) 654-658.

[17] M. F. Dupont, D. R. MacFarlane, J. M. Pringle, Thermo-electrochemical cells for waste heat harvesting – progress and perspectives, Chem. Commun. 53 (2017) 6288-6302.

[18] J. Duan, B. Yu, L. Huang, B. Hu, M. Xu, G. Feng, J. Zhou, Liquid-state thermocells: Opportunities and challenges for low-grade heat harvesting, Joule 5 (2021) 768-779.

[19] S. L. Kim, H. T. Lin, C. Yu, Thermally chargeable solid-state supercapacitor, Adv. Energy Mater. 6 (2016) 1600546.

[20] A. Sohn, C. Yu, Ionic transport properties and their empirical correlations for thermal-to-electrical energy conversion, Mater. Today Phys. 19 (2021) 100433.

[21] Y. Zhang, A. Sohn, A. Chakraborty, C. Yu, Colossal thermo-hydro-electrochemical voltage generation for self-sustainable operation of electronics, Nat. Commun. 12 (2021) 5269.

[22] S. W. Lee, Y. Yang, H. W. Lee, H. Ghasemi, D. Kraemer, G. Chen, Y. Cui, An electrochemical system for efficiently harvesting low-grade heat energy, Nat. Commun. 5 (2014) 3942.

[23] C. Gao, S. W. Lee, Y. Yang, Thermally regenerative electrochemical cycle for low-grade heat harvesting, ACS Energy Lett. 2 (2017) 2326-2334.

[24] A. Abdollahipour, H. Sayyaadi, A review of thermally regenerative electrochemical systems for power generation and refrigeration applications, Appl. Therm. Eng. 187 (2021) 116576.

[25] C. Cheng, Y. Dai, J. Yu, C. Liu, S. Wang, S.-P. Feng, M. Ni, Review of liquid-based systems to recover low-grade waste heat for electrical energy generation, Energy Fuels 35 (2021) 161-175.

[26] C. Gao, Y. Liu, L. Zheng, E. Feng, S. Sim, Y. Kim, J. Yun, M. Kim, S. W. Lee, The Effect of electrolyte type on the Li ion intercalation in copper hexacyanoferrate, J. Electrochem. Soc. 166 (2019) A1732-A1737.

[27] C. Gao, Y. Liu, B. Cheng, J. Yun, E. Feng, Y. Kim, M. Kim, A. Choi, H.-W. Lee, S. W. Lee, Efficient low-grade heat harvesting enabled by tuning the hydration entropy in an electrochemical system, Adv. Mater. 33 (2021) 2004717.

[28] C. Gao, Y. Yin, L. Zheng, Y. Liu, S. Sim, Y. He, C. Zhu, Z. Liu, H.-W. Lee, Q. Yuan, S. W. Lee, Engineering the electrochemical temperature coefficient for efficient low-grade heat harvesting, Adv. Funct. Mater. 28 (2018) 1803129.

[29] Y. Liu, C. Gao, S. Sim, M. Kim, S. W. Lee, Lithium manganese oxide in an aqueous electrochemical system for low-grade thermal energy harvesting, Chem. Mater. 31 (2019) 4379-4384.

[30] C. Cheng, S. Wang, P. Tan, Y. Dai, J. Yu, R. Cheng, S.-P. Feng, M. Ni, Insights into the thermopower of thermally regenerative electrochemical cycle for low grade heat harvesting, ACS Energy Lett. 6 (2020) 329-336.

[31] H. Zhang, F. Zhang, J. Yu, M. Zhou, W. Luo, Y. M. Lee, M. Si, Q. Wang, Redox targeting-based thermally regenerative electrochemical cycle flow cell for enhanced low-grade heat harnessing, Adv. Mater. 2020, 2006234.

[32] J. Jiang, H. Tian, X. He, Q. Zeng, Y. Niu, T. Zhou, Y. Yang, C. Wang, A CoHCF system with enhanced energy conversion efficiency for low-grade heat harvesting, J. Mater. Chem. A 7 (2019) 23862-23867.

[33] Y. Yang, J. Loomis, H. Ghasemi, S. W. Lee, Y. J. Wang, Y. Cui, G. Chen, Membrane-free battery for harvesting low-grade thermal energy, Nano Lett. 14 (2014) 6578-6583.

[34] Y. Yang, S. W. Lee, H. Ghasemi, J. Loomis, X. Li, D. Kraemer, G. Zheng, Y. Cui, G. Chen, Charging-free electrochemical system for harvesting low-grade thermal energy, Proc. Natl. Acad. Sci. U. S. A. 111 (2014) 17011-17016.

[35] R. Long, B. Li, Z. Liu, W. Liu, Performance analysis of a dual loop thermally regenerative electrochemical cycle for waste heat recovery, Energy 107 (2016) 388-395.

[36] A. D. Poletayev, I. S. McKay, W. C. Chueh, A. Majumdar, Continuous electrochemical heat engines, Energy Environ. Sci. 11 (2018) 2964-2971.

[37] R. Hu, B. A. Cola, N. Haram, J. N. Barisci, S. Lee, S. Stoughton, G. Wallace, C. Too, M. Thomas, A. Gestos, M. E. dela Cruz, J. P. Ferraris, A. A. Zakhidov, R. H. Baughman, Harvesting waste thermal energy using a carbon-nanotube-based thermo-electrochemical cell, Nano Lett. 10 (2010) 838-846.

[38] M. S. Romano, N. Li, D. Antiohos, J. M. Razal, A. Nattestad, S. Beirne, S. Fang , Y. Chen, R. Jalili, G. G. Wallace, R. Baughman, Carbon nanotube – Reduced graphene oxide composites for thermal energy harvesting applications, J. Chen, Adv. Mater. 25 (2013) 6602-6606.

[39] H. Im, T. Kim, H. Song, J. Choi, J. S. Park, R. Ovalle-Robles, H. D. Yang, K. D. Kihm, R. H. Baughman, H. H. Lee, T. J. Kang, Y. H. Kim, High-efficiency electrochemical thermal energy harvester using carbon nanotube aerogel sheet electrodes, Nat. Commun. 7 (2016) 10600.

[40] L. Zhang, T. Kim, N. Li, T. J. Kang, J. Chen, J. M. Pringle, M. Zhang, A. H. Kazim, S. Fang, C. Haines, D. Al-Masri, B. A. Cola, J. M. Razal, J. Di, S. Beirne, D. R. MacFarlane, A. Gonzalez-Martin, S. Mathew, Y. H. Kim, G. Wallace, R. H. Baughman, High power density electrochemical thermocells for inexpensively harvesting low-grade thermal energy, Adv. Mater. 29 (2017) 1605652.

[41] B. Yu, J. Duan, H. Cong, W. Xie, R. Liu, X. Zhuang, H. Wang, B. Qi, M. Xu, Z. L. Wang, J. Zhou, Thermosensitive crystallization-boosted liquid thermocells for low-grade heat harvesting, Science 370 (2020) 342-346.

[42] A. P. Straub, N. Y. Yip, S. H. Lin, J. Lee, M. Elimelech, Harvesting low-grade heat energy using thermo-osmotic vapour transport through nanoporous membranes, Nat. Energy, 1 (2016) 16090.

[43] X. Wang, Y.-T. Huang, C. Liu, K. Mu, K. H. Li, S. Wang, Y. Yang, L. Wang, C.-H. Su, S.-P. Feng, Direct thermal charging cell for converting low-grade heat to electricity, Nat. Commun. 10 (2019) 4151.

[44] F. Zhang, J. Liu, W. Yang, B. E. Logan, A thermally regenerative ammonia-based battery for efficient harvesting of low-grade thermal energy as electrical power, Energ. Environ. Sci. 8 (2015) 343-349.

[45] F. Zhang, N. La Barge, W. Yang, J. Liu, B. E. Logan, Enhancing low-grade thermal energy recovery in a thermally regenerative ammonia battery using elevated temperatures, ChemSusChem 8 (2015) 1043-1048.

[46] M. Rahimi, L. Zhu, K. L. Kowalski, X. Zhu, C. A. Gorski, M. A. Hickner, B. E. Logan, Improved electrical power production of thermally regenerative batteries using a poly(phenylene oxide) based anion exchange membrane, J. Power Sources 342 (2017) 956-963.

[47] X. Zhu, M. Rahimi, C. A. Gorski, B. Logan, A thermally-regenerative ammonia-based flow battery for electrical energy recovery from waste heat, ChemSusChem 9 (2016) 873-879.

[48] M. Rahimi, T. Kim, C. A. Gorski, B. E. Logan, A thermally regenerative ammonia battery with carbon-silver electrodes for converting low-grade waste heat to electricity, J. Power Sources 373 (2018) 95-102.

[49] W. Wang, G. Shu, H. Tian, D. Huo, X. Zhu, A bimetallic thermally-regenerative ammonia-based flow battery for low-grade waste heat recovery, J. Power Sources 424 (2019) 184-192.

[50] W. Wang, G. Shu, X. Zhu, H. Tian, Decoupled electrolytes towards enhanced energy and high temperature performance of thermally regenerative ammonia batteries, J. Mater. Chem. A 8 (2020) 12351-12360.

[51] M. Rahimi, A. D'Angelo, C. A. Gorski, O. Scialdone, B. E. Logan, Electrical power production from low-grade waste heat using a thermally regenerative ethylenediamine battery, J. Power Sources, 351 (2017) 45-50.

[52] A. D. Poletayev, I. S. McKay, W. C. Chueh, A. Majumdar, Continuous electrochemical heat engines, Energy Environ. Sci. 11 (2018) 2964-2971.

[53] I. Facchinetti, R. Ruffo, F. La Mantia, D. Brogioli, Thermally regenerable redox flow battery for exploiting low-temperature heat sources, Cell Rep. Phys. Science 1 (2020) 100056.

[54] N. Y. Yip, M. Elimelech, Comparison of energy efficiency and power density in pressure retarded osmosis and reverse electrodialysis, Environ. Sci. Technol. 48 (2014) 11002-11012.

[55] X. Zhu, W. He, B. E. Logan, Influence of solution concentration and salt types on the performance of reverse electrodialysis cells, J. Membr. Sci. 494 (2015) 154-160.

[56] S. Maye, H. H. Girault, P. Peljo, Thermally regenerative copper nanoslurry flow batteries for heat-to-power conversion with low-grade thermal energy, Energy Environ. Sci. 13 (2020) 2191-2199.